1 mM ascorbic acid in all buffers.

15. Changes in the plasma membrane potential were monitored by measurement of changes in the intensity of fluorescence emission of the dye 3,3′ dipropylthiadicarbocyanine iodide [DiS-C_3-(5)], which is sensitive to membrane potential (*12*). The assay medium was 20 mM MES (pH 5.5), 370 mM sorbitol, 20 mM KCl, 1 mM $CaCl_2$, 90 mM sucrose, and 10^5 protoplasts per milliliter. The dye DiS-C_3-(5) was added to the assay medium to a final concentration of 2 μM, and the suspension was incubated at 25°C for 1 hour (in the experiments monitoring circadian rhythmicity) or for 5 min (in the experiments monitoring light sensitivity). As an antioxidant, 0.2 mM DTT was included to protect the dye during the hour-long incubations. Excitation of the dye was at 620 nm and emission was measured at 668 nm.
16. To demonstrate that the failure of added K^+ to depolarize unresponsive protoplasts did not result from a loss of membrane integrity, we incubated the protoplasts with valinomycin and 200 mM K^+. Depolarization induced by the ionophore plus K^+ demonstrated that the protoplasts were intact (*12*).
17. White light was provided with Sylvania GTE fluorescent bulbs (32 W, 4100K). Photon fluence rate, as measured with an L1-170 Quantum Meter (Li-Corp.) or an 818 series photodetector (Newport Corp.), was 20 μmol m^{-2} s^{-1}.
18. After 21 hours the protoplasts began to lose viability, preventing observations of further cycles.
19. We provided red and far-red light pulses by filtering the output of a fiber-optic lamp (Reichart Scientific Instruments, Buffalo, NY) through a heat-reflecting filter (Corion #HR750-F1-L255) and appropriate interference filters. The red filter was Oriel Optics no. 53960 and the far-red filter was Oriel Optics no. 53985. Peak transmittance was at 660 nm for red and 725 nm for far-red, with half-bandwidths of 10 nm in each case. The fluence rate was 80 μmol m^{-2} s^{-1} for red pulses and 40 μmol m^{-2} s^{-1} for far-red pulses.
20. Three-minute irradiation with white light was performed as in (*17*). Similar irradiation with red light was as in (*19*) except that the fluence rate was 3 to 4 μmol m^{-2} s^{-1}. Irradiation with high-intensity red light could not be continued beyond 60 s because the potential-sensitive dye was bleached by continued illumination, even in the absence of protoplasts. Blue light irradiation was as described previously (*12*) at a fluence rate of 3 to 4 μmol m^{-2} s^{-1}. The blue filters that were used transmitted significantly above 730 nm, in the absorbance range of the far-red–absorbing form of phytochrome. However, the blue filters were always used in combination with the heat reflecting filters, and transmittance by the combined filters was <1% at all wavelengths from 600 to 800 nm (red and far-red range).
21. We thank the University of Connecticut Biotechnology Center for the use of a fluorescence spectrophotometer. Supported by National Science Foundation grants DCB 8905259 and IBN 9206179 and U.S.–Israel Binational Agricultural Research and Development Fund grant IS-1670-90RC (R.C.C.).

16 November 1992; accepted 23 February 1993

A Large Drop in Atmospheric $^{14}C/^{12}C$ and Reduced Melting in the Younger Dryas, Documented with ^{230}Th Ages of Corals

R. Lawrence Edwards,* J. Warren Beck, G. S. Burr, D. J. Donahue, J. M. A. Chappell, A. L. Bloom, E. R. M. Druffel, F. W. Taylor

Paired carbon-14 (^{14}C) and thorium-230(^{230}Th) ages were determined on fossil corals from the Huon Peninsula, Papua New Guinea. The ages were used to calibrate part of the ^{14}C time scale and to estimate rates of sea-level rise during the last deglaciation. An abrupt offset between the ^{14}C and ^{230}Th ages suggests that the atmospheric $^{14}C/^{12}C$ ratio dropped by 15 percent during the latter part of and after the Younger Dryas (YD). This prominent drop coincides with greatly reduced rates of sea-level rise. Reduction of melting because of cooler conditions during the YD may have caused an increase in the rate of ocean ventilation, which caused the atmospheric $^{14}C/^{12}C$ ratio to fall. The record of sea-level rise also shows that globally averaged rates of melting were relatively high at the beginning of the YD. Thus, these measurements satisfy one of the conditions required by the hypothesis that the diversion of meltwater from the Mississippi to the St. Lawrence River triggered the YD event.

Carbon-14 dating requires prior knowledge of secular variations in the atmospheric $^{14}C/^{12}C$ ratio (*1*). This ratio changes in response to shifts in the intensity of the solar or terrestrial magnetic fields, which modulate incoming cosmic rays responsible for atmospheric ^{14}C production. Changes in the atmospheric $^{14}C/^{12}C$ ratio may also result from redistribution of carbon of different isotopic compositions among the various carbon reservoirs. Detailed records of atmospheric $^{14}C/^{12}C$ have been obtained for the last 11,000 years from measurements of carbon in wood, where annual tree rings provide an independent chronology for the establishment of variations in the atmospheric $^{14}C/^{12}C$ ratio (*2–4*). However, extension of the record to earlier times has been hindered by lack of an appropriate absolute chronometer.

As early as 1965, Kaufman and Broecker (*5*) used ^{230}Th dating of carbonates for absolute time control in ^{14}C calibration. The early measurements constrained the past atmospheric $^{14}C/^{12}C$ ratio, but detailed records were not possible because alpha-counting measurements of ^{234}U and ^{230}Th were not sufficiently precise. In recent years, the development of thermal ionization mass spectrometric (TIMS) methods for the measurement of ^{234}U (*6*) and ^{230}Th (*7*) resulted in large increases in analytical precision and sensitivity. By the application of TIMS measurements to fossil corals, Edwards and colleagues (*7*) obtained ^{230}Th ages that were more precise than ^{14}C ages. This breakthrough made it possible to calibrate the ^{14}C chronometer with combined ^{230}Th age determinations and $^{14}C/^{12}C$ analyses. Fairbanks (*8*) recovered the first sequence of appropriate age for the extension of the atmospheric $^{14}C/^{12}C$ record by underwater drilling off the coast of Barbados. This sequence showed large offsets between ^{14}C and ^{230}Th ages (*9*), which suggests that the atmospheric $^{14}C/^{12}C$ ratio was high about 20,000 years ago. The subsequent drop in the atmospheric $^{14}C/^{12}C$ ratio was originally attributed to an increase in the terrestrial magnetic-field strength. However, Stuiver and co-workers (*10*) have raised questions about the Barbados data because this record disagrees with $^{14}C/^{12}C$ records from some varved lake sediments.

The same Barbados corals show a record of sea-level rise during the last deglaciation (*8*). Their depth and age relationships suggest that the rise was characterized by two meltwater pulses separated by a period of reduced melting (PRM). The timing of the PRM has implications for the cause of the Younger Dryas (YD), an interval of time during deglaciation when the climate in northern Europe returned to near-glacial conditions. However, Broecker (*11*) has questioned the record because the inferred meltwater pulses occurred at core breaks.

In this report, we present a new coral record derived from a single drill core from the Huon Peninsula, Papua New Guinea. This record has similarities to the Barbados record but also important differences, which have implications regarding the calibration of the ^{14}C time scale, the cause of a large decrease in the atmospheric $^{14}C/^{12}C$

R. L. Edwards and J. W. Beck, Minnesota Isotope Laboratory, Department of Geology and Geophysics, University of Minnesota, Minneapolis, MN 55455.
G. S. Burr and D. J. Donahue, Department of Physics, National Science Foundation Accelerator Facility for Radioisotope Analysis, University of Arizona, Tucson, AZ 85721.
J. M. A. Chappell, Department of Biogeography and Geomorphology, Research School of Pacific Studies, Australian National University, Canberra, ACT 2601, Australia.
A. L. Bloom, Department of Geological Sciences, Cornell University, 2122 Snee Hall, Ithaca, NY 14853.
E. R. M. Druffel, Department of Marine Chemistry and Geochemistry, Woods Hole Oceanographic Institution, Woods Hole, MA 02543.
F. W. Taylor, Institute for Geophysics, University of Texas at Austin, Austin, TX 78759.
*To whom correspondence should be addressed.

ratio, the rate of sea-level rise during deglaciation, and the cause of the YD. Most of the New Guinea samples are from a drill site 5 km southeast of the village of Sialum (*12*). The top of the core is 6 m above sea level, and the base is 46 m below sea level. When this record is corrected for tectonic uplift (*13*), the core represents material that grew while sea level was rising from 71 to 8 m below the present sea level. Several common shallow-water coral genera, mostly *Porites* sp., were analyzed. Additional, previously reported ^{14}C ages showed that the core ranges in age from 7,000 to 11,000 ^{14}C years old (*12, 14*).

For small samples, $^{14}C/^{12}C$ ratios were measured by accelerator mass spectrometry at the University of Arizona (*15–18*). Samples larger than 20 g were analyzed by high-precision, conventional-gas proportional counting of acetylene gas at Woods Hole Oceanographic Institution (*18, 19*). A key aspect of the procedure in both laboratories is the addition of a selective dissolution step, which removes potential contamination. Diagenetic processes can add significant amounts of carbon with high $^{14}C/^{12}C$ ratios to corals (*17, 20, 21*), but selective dissolution techniques can remove such natural contaminants (*17*). Selective dissolution was not used in the original Barbados ^{14}C calibration (*9*) but was applied later (*22*). The $^{14}C/^{12}C$ values for selectively dissolved samples from the latter data set are generally lower than the original ones (*21*), which suggests that the latter data are more reliable. Consequently further reference to the Barbados ^{14}C data in this report is restricted to the selectively dissolved samples in (*22*).

We were also concerned about potential inaccuracies in ^{230}Th ages. Corals with ages that are known independently, from annual

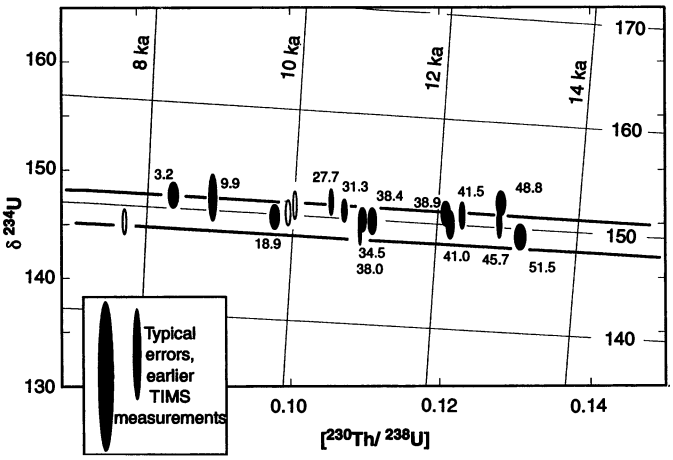

Fig. 1. Measured $\delta^{234}U$ versus the $^{230}Th/^{238}U$ activity ratio, contoured in ^{230}Th age (subvertical lines) and initial $\delta^{234}U$ (subhorizontal curves). The two bold initial $\delta^{234}U$ contours represent the range of possible $\delta^{234}U$ values for surface seawater (149.7 ± 1.5). Each data point is represented by a 2σ error ellipse (open ellipses, surface samples; filled ellipses, drill-core samples). The inset shows typical errors for earlier mass spectrometric measurements [ellipse on right from (*7*), ellipse on left from (*9*)]. Compared with these two examples, our $\delta^{234}U$ errors are smaller, an important factor in the identification of material that may have exchanged small amounts of uranium. All points plot within the range of surface seawater, consistent with closed-system evolution and accurate ages. Possible glacial-interglacial variations in marine uranium isotopic composition are less than 2 per mil. Numbers adjacent to ellipses represent depths in the core (in meters below the surface at the drilling site). The ^{230}Th ages increase with depth, consistent with accurate ages.

Table 1. Data for U, Th, and C isotopes; ^{14}C and ^{230}Th ages. The last significant figures of the 2σ errors are in parentheses. The ^{14}C analyses were made at Arizona except those labeled w, which were made at Woods Hole.

Sample*		^{238}U (μg/g)	^{232}Th (pg/g)	$\delta^{234}U$† measured	$\delta^{234}U$† initial	$[^{230}Th/^{238}U]$	^{230}Th age‡ (years B.P.)	^{14}C age§ (years B.P.)	$\Delta^{14}C$‖ (per mil)
HOB-EE-5	a	2.661 (2)	68 (2)	149.0 (1.4)	149.8 (1.5)	0.01938 (9)	1808 (9)	1920 (100)	−20 (11)
	b	2.647 (1)	42 (1)	149.7 (1.3)	150.4 (1.3)	0.01908 (8)	1779 (9)	1850 (40)w	−15 (5)
KAI-EE-1	a	2.707 (2)	74 (2)	148.8 (1.2)	149.8 (1.2)	0.02500 (10)	2350 (11)	2490 (110)	−25 (13)
	b							2430 (70)w	−18 (8)
KAI-BB-3	a	2.411 (1)	115 (4)	145.3 (1.1)	148.5 (1.2)	0.07837 (26)	7656 (28)	7230 (80)	26 (10)
	b			143.3 (1.1)				7110 (80)w	42 (11)
HOB-EE-3	a	2.302 (2)	48 (8)	146.1 (1.1)	150.3 (1.1)	0.09992 (42)	9860 (44)	8940 (110)	83 (15)
	b			146.3 (1.2)				8980 (90)w	79 (13)
HOB-EE-1	a	2.455 (1)	35 (3)	146.8 (1.2)	151.0 (1.3)	0.10086 (26)	9951 (29)	8880 (120)	103 (17)
	b			144.8 (1.3)				8940 (90)w	96 (13)
3.2		2.653 (1)	745 (12)	147.8 (1.1)	151.3 (1.2)	0.08550 (69)	8363 (71)	7550 (140)	74 (20)
9.9		2.875 (2)	290 (9)	147.6 (2.2)	151.3 (2.2)	0.08936 (46)	8760 (51)	7750 (270)	100 (36)
18.9		3.373 (2)	178 (11)	145.4 (1.2)	149.5 (1.2)	0.09776 (69)	9642 (72)	8730 (120)	84 (18)
27.7		2.578 (2)	154 (6)	147.2 (1.3)	151.7 (1.3)	0.10609 (73)	10490 (77)	9300 (140)	118 (19)
31.3		3.279 (2)	109 (5)	146.4 (1.1)	150.9 (1.2)	0.10777 (21)	10673 (25)	9530 (120)	109 (17)
34.5		3.136 (1)	367 (11)	145.1 (1.2)	149.7 (1.2)	0.11035 (50)	10955 (54)	9790 (120)	112 (17)
38.0	a	3.441 (1)	106 (2)	144.4 (1.3)	148.9 (1.4)	0.10985 (22)	10912 (27)	10090 (80)	66 (11)
	b	3.140 (1)		143.7 (1.4)					
38.4		3.215 (2)	330 (5)	145.2 (1.2)	149.9 (1.3)	0.11122 (53)	11045 (57)	9990 (90)	97 (14)
38.9		2.484 (1)	544 (7)	146.2 (1.7)	151.3 (1.7)	0.12120 (64)	12084 (70)	10430 (140)	178 (20)
41.0		2.362 (1)	86 (10)	144.5 (1.4)	149.6 (1.4)	0.12169 (51)	12155 (56)	10410 (120)	190 (18)
41.5		3.389 (3)	316 (7)	145.5 (0.9)	150.7 (0.9)	0.12346 (36)	12332 (39)	10200 (130)	247 (20)
45.7		3.482 (2)	94 (4)	145.0 (1.6)	150.4 (1.6)	0.12798 (30)	12818 (37)		
48.8		3.130 (2)	318 (6)	146.9 (1.2)	152.3 (1.2)	0.12838 (63)	12837 (68)	10980 (110)	204 (17)
51.5		3.527 (2)	2209 (11)	143.8 (1.2)	149.3 (1.2)	0.13077 (78)	13129 (84)	10970 (110)	249 (18)

*Numbered samples are from the drill core; numbers indicate the depth in meters below the surface, which is 6 m above sea level. Uppercase letters indicate samples collected from surface exposures. Lowercase letters indicate duplicate analyses of different pieces of the same coral. †See (*27*). ‡The ^{230}Th ages are calculated from the equation

$$[^{230}Th/^{238}U] - 1 = -e^{-\lambda_{230}T} + (\delta^{234}U_m/1000)[\lambda_{230}/(\lambda_{230} - \lambda_{234})](1 - e^{(\lambda_{234}-\lambda_{230})T})$$

where λ's are the respective decay constants (*49*), $\delta^{234}U_m$ is the measured $\delta^{234}U$ value (*27*), $[^{230}Th/^{238}U]$ is the $^{230}Th/^{238}U$ activity ratio, and T is the age. §Conventional ^{14}C age calculated with the 5568 half-life. The magnitude of the reservoir effect (407 ± 52 years, 49.4 ± 6.6 per mil) was calculated from sample HOB-EE-5b as described in the text; this value has been subtracted from each age. The error in the reservoir effect is included in the quoted error for each age, except for HOB-EE-5b. ‖See(*30*).

growth bands and ^{14}C dating, demonstrate that ^{230}Th ages are accurate for carefully selected samples younger than 8000 years old (*7*, 9). However, some corals older than several tens of thousands of years have initial $^{234}U/^{238}U$ ratios greater than modern marine values. Thus, exchange of uranium may have occurred after skeletal growth (*7*, *23*, *24*). To increase sensitivity in detecting uranium of diagenetic origin, we modified (*25*) procedures (6, *7*) to increase further the precision with which the $^{234}U/^{238}U$ ratio can be measured. Measurements were made at the University of Minnesota on a Finnigan MAT 262 RPQ thermal ionization mass spectrometer. Eight measurements of $^{234}U/^{238}U$ in New Brunswick Laboratories (NBL) Standard Reference Material 112a (*26*) gave a mean $^{234}U/^{238}U$ value of $52.854 \times 10^{-6} \pm 0.066 \times 10^{-6}$, which corresponds to a $\delta^{234}U$ value (*27*) of -34.1 ± 1.2 per mil, where the error is the external error (2σ of the population of the eight measurements). The external and counting-statistics errors are similar, indicating that the only significant source of imprecision is from counting statistics. The $^{234}U/^{238}U$ value agrees with earlier determinations (6, *28*); however, precisions are higher, which is important for the detection of samples that may have exchanged small amounts of uranium (Fig. 1).

Initial $\delta^{234}U$ values (*27*) for two young Huon Peninsula corals collected from surface exposures (HOB-EE-5 and KAI-EE-1 in Table 1) agree with the value for a young (132 ± 3 years) sample from Barbados (*24*). The agreement of the initial values from different oceans suggests that spacial variations in the $^{234}U/^{238}U$ ratio of open-ocean surface seawater are not resolvable. The mean of 149.7 ± 1.5 per mil (2σ) for the two Huon Peninsula samples and one Barbados sample gives a precise $\delta^{234}U$ value for surface seawater. Initial $\delta^{234}U$ values of all other samples (Fig. 1 and Table 1) are indistinguishable, at a precision of ± 1 per mil, from this value. Thus, the data show no evidence for diagenetic exchange of uranium. The initial $^{234}U/^{238}U$ values show that the marine $^{234}U/^{238}U$ ratio varied by no more than 2 per mil in the last 13,000 years. This interval is just the period over which one would expect possible glacial-interglacial shifts in uranium isotopic composition of the sort that were recently documented for the $^{87}Sr/^{86}Sr$ ratio (*29*). Because none were observed, any shifts must have been smaller than 2 per mil.

The difference between the $^{14}C/^{12}C$ ratio of the atmosphere and that of the surface seawater (the reservoir effect) near the drill site was established by analysis of a surface sample (HOB-EE-5b in Table 1). The $\Delta^{14}C$ value (*30*, *31*) at the time the coral grew was calculated from the measured $^{14}C/^{12}C$ ratio and the ^{230}Th age. The difference between the known atmospheric $^{14}C/^{12}C$ ratio (*2*, *32*) at the time of growth and the initial value for the coral is 49.4 ± 6.6 (2σ) per mil, equivalent to a difference in radiocarbon age of 407 ± 52 years. This value is consistent with previous estimates for the Huon Peninsula reservoir effect (*12*) as well as the estimate from KAI-EE-1, another coral that grew within the period for which the atmospheric $^{14}C/^{12}C$ ratio is known from dendrochronology (Table 1). This correction has been subtracted from all of our ^{14}C ages.

For drill-core samples, ^{14}C ages range between 6530 ± 110 (2σ) and $10,970 \pm 110$ years B.P. (*14*) for coral that grew while the sea level rose from 71 to 8 m below the present sea level (*13*) (Fig. 2). The ages are similar to those previously reported for different samples from the same core (*12*). The rise in sea level inferred from our ^{14}C curve is also similar to the value from the Barbados curve (*8*, *12*). However, the Huon curve shows no evidence for slower sea-level rise during and before the YD, as does the Barbados ^{14}C curve. The ^{230}Th ages for core samples range from $8,363 \pm 71$ to $13,129 \pm 84$ years B.P. for coral that grew while the sea level rose from 71 to 14 m below its present height (*13*) (Fig. 2). The ages increase progressively with depth, as do the accurate values, and no genera-related discrepancies in age were noted. In contrast to the ^{14}C curve, the ^{230}Th curve shows dramatic evidence for slower sea-level rise between $12,332 \pm 39$ and $11,045 \pm 57$ years B.P. (*14*) (between $10,200 \pm 130$ and $9,990 \pm 90$ ^{14}C years B.P.). The rate of upward reef growth, and the presumed rate of sea-level rise, decreased from as rapid as 16 m per thousand years before this interval to 2 m per thousand years during the interval and then increased immediately after the interval to rates as high as 28 m per thousand years (Fig. 3). This pattern supports the idea that deglaciation was punctuated by at least one PRM (*8*, *33*). Unlike that of the Barbados curve, the PRM recorded in the Huon Peninsula core was shorter, younger, and characterized by a lower melt rate. The discrepancies may reflect differences in sample density, potential artifacts associated with core breaks, potential downslope movement of corals, or corals that grew at significant but variable depths below sea level. The relatively high melt rate for the PRM recorded at Barbados is in part an artifact because the original Barbados meltwater curve (*8*) was based on ^{14}C dates. The ^{14}C time scale is now known to be highly compressed at about 10,000 ^{14}C

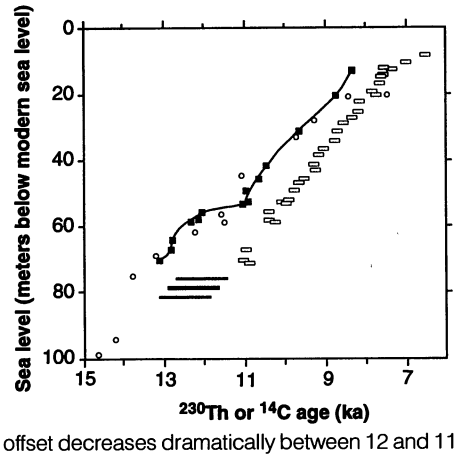

Fig. 2. Plot of ^{14}C (open rectangles) and ^{230}Th ages (filled boxes) versus initial depth for Papua New Guinea drill-core samples. Also shown are Barbados ^{230}Th data (open circles) (*9*). For the Papua New Guinea data, the width of each symbol is less than or equal to the 2σ error in age. Initial depth is calculated from the present elevation as described in (*13*). The three horizontal bars represent the timing of the YD in calendar years (*35*): top bar, latest possible timing, with errors taken into consideration; middle bar, best estimate of timing; and bottom bar, earliest possible timing. The ^{230}Th curve shows strong evidence for a PRM that started at or after the onset of the YD and ended several hundred years after its end. The deepest samples have large offsets (2000 years) between ^{14}C and ^{230}Th ages, which indicate high atmospheric $^{14}C/^{12}C$. The offset decreases dramatically between 12 and 11 ka, which indicates rapidly falling atmospheric $^{14}C/^{12}C$.

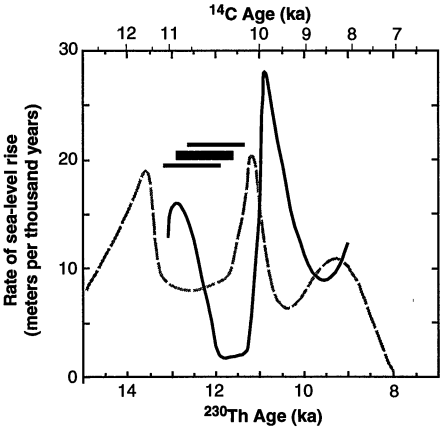

Fig. 3. Rate of sea-level rise as a function of time, derived by differentiation of the curve in Fig. 2. The black curve is the Papua New Guinea data. The dashed trace is a similar curve for Barbados, derived from (*9*). Both curves are based on ^{230}Th ages. Time is in ^{230}Th years (presumably equivalent to calendar years) on the lower *x* axis, and in conventional ^{14}C years on the upper *x* axis, on the basis of the calibration in Fig. 4 and (*22*). The horizontal bars represent the timing of the YD (*35*) (see caption for Fig. 2). Both curves show a period of reduced melting, but the Papua New Guinea data suggest that the melt rate was lower and that reduced melting started later.

years ago (8 and below), which has led to the calculation of artificially high melt rates. Even if the Barbados curve is recalculated with ^{230}Th dates (Fig. 3), it still gives a relatively high melt rate for the PRM. More refined studies may ultimately resolve these discrepancies. In support of the Huon Peninsula record, the most prominent feature in the sea-level curve is the PRM, which coincides with the most prominent feature in the $^{14}C/^{12}C$ curve. We defend this relationship as more than coincidental.

Knowledge of the temporal relationship between the PRM and the YD helps to distinguish between hypotheses regarding the cause of the YD. It has been hypothesized that diversion of meltwater from the Mississippi into the St. Lawrence River caused the YD by lowering the salinity of North Atlantic surface water (*34*). Low-density surface water hindered the convective sinking of North Atlantic Deep Water (NADW). Because NADW sinking is responsible for meridonal heat transport to the North Atlantic, a lower rate of NADW formation resulted in cooler conditions during the YD. The Barbados chronology does not support this idea because it implies that the PRM started before and continued throughout the YD (*8*, *35*). A low melt rate that began before the YD would not have allowed formation of the low salinity cap required by the meltwater-diversion hypothesis. In contrast, our data (Figs. 2 and 3) suggest that the rise in sea level slowed after the onset of the YD and increased again several hundred years after its end. This discrepancy between the Barbados and Huon Peninsula data is critical. Because our data indicate high melt rates at the start of the YD, they suggest that meltwater input or diversion is a plausible trigger for the YD. Our data show that the melt rate fell to its lowest value during the YD. Therefore, one must determine another mechanism beside the continued input of low-density meltwater to explain the cool climate toward the end of the YD. The reduced melting after the onset of the YD would appear to be a response to cooling during the YD rather than a phenomenon that is necessarily related to the cause of the YD.

For three of four samples within the range for which ^{14}C is well calibrated (*2*, *3*), our combined ^{230}Th and ^{14}C data agree with the established dendrochronology, consistent with accurate ages and a temporally constant reservoir effect (Table 1 and Figs. 4 and 5). Values for the fourth point (KAI-BB-3) are slightly off the calibration, a discrepancy that we do not understand. Data for all eight samples with ages that lie within the range for which ^{14}C is calibrated with a floating chronology (*4*) agree with the calibration, which makes them consistent with accurate ages, a constant reservoir effect, and accurate placement of the floating chronology. For parts of the curve between 13 and 11 thousand years ago (ka), a period for which no dendrochronological calibration is available, the data offer sev-

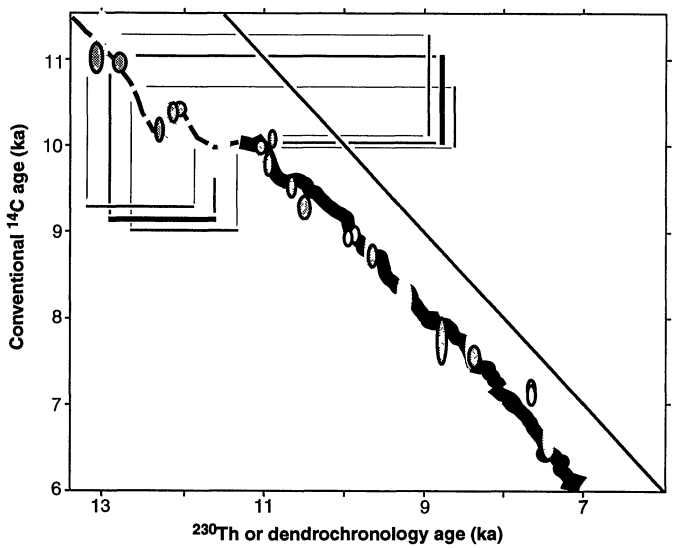

Fig. 4. Plot of ^{14}C versus ^{230}Th ages. Ellipses with black outlines are Papua New Guinea data. Of these, stipled ellipses are University of Arizona ^{14}C analyses and open ellipses are Woods Hole ^{14}C analyses. Stipled ellipses with no outline are Barbados data (*22*). The thick black curve represents established and floating dendrochronological ^{14}C calibrations (*2–4*). The horizontal bars indicate the timing of the YD, in calendar years, from ice cores (*35*). The middle horizontal bar is the best estimate of the timing; with errors taken into consideration, the upper horizontal bar is the oldest possible timing and the lower bar is the youngest possible timing. The vertical bars represent corresponding estimates of the timing of the YD in ^{14}C years, on the basis of the ice-core data and our calibration. The best and the earliest possible estimates agree with other radiocarbon-based estimates of the timing of the YD (*35*), suggesting that the calibration is accurate. The latest possible estimate for the start of the YD is later than other radiocarbon-based estimates, which suggests that the latest possible ice-core estimate is too young. The Papua New Guinea data define a 1280-year interval between 12.3 and 11.0 ka over which ^{14}C ages changed by only 210 years. This period was coincident with the period of reduced melting (Figs. 2 and 3). A decrease in atmospheric $^{14}C/^{12}C$ (Fig. 5) caused the compression of the ^{14}C time scale during this period.

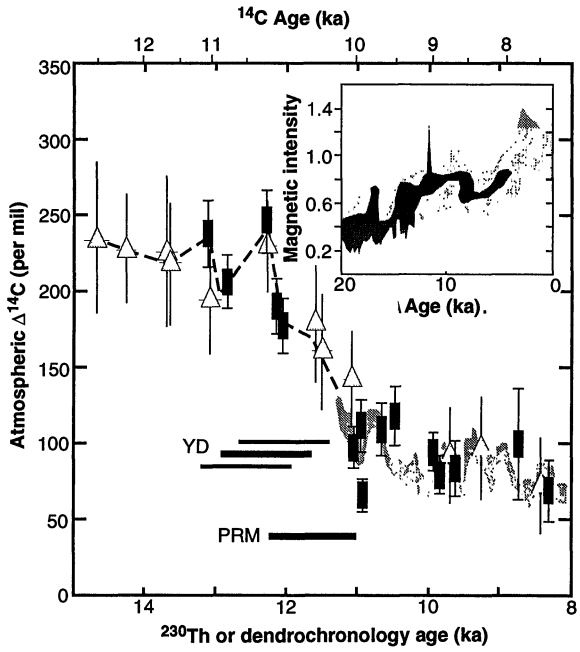

Fig. 5. Atmospheric $\Delta^{14}C$ between 15 and 8 ka. The inset shows a record of the intensity of the Earth's magnetic dipole (*39*). Time is in ^{230}Th years (presumably equivalent to calendar years) on the lower *x* axis and in conventional ^{14}C years on the upper *x* axis [on the basis of the calibration in Fig. 4 and (*22*)]. Solid boxes are Papua New Guinea data; triangles are Barbados data (*22*). The stippled curve is based on dendrochronology (*2–4*). The dashed curve is a spline drawn through the coral data, which are consistent with each other and generally consistent with the dendrochronology. The bars labeled YD represent the timing of the YD on the basis of ice-core data (*35*): upper bar, latest possible timing; middle bar, best estimate; and lower bar, earliest possible timing. The other bar represents the timing of the PRM from the Huon Peninsula core (Figs. 2 and 3). The Papua New Guinea data show a rapid decrease in $\Delta^{14}C$ between 12.3 and 11.0 ka, which is the most prominent feature yet identified in records of atmospheric $\Delta^{14}C$ and is synchronous with the PRM. This decrease represents almost two-thirds of the total decrease in $\Delta^{14}C$ between 19 and 11 ka. A large portion of the $\Delta^{14}C$ decrease may have been caused by changes in the cycling of carbon in the ocean.

eral inferences. At 13,130 years B.P., ^{14}C ages are 2,160 years younger than ^{230}Th ages, corresponding to an atmospheric $\Delta^{14}C$ of 249 ± 18 per mil (30). At 12,330 years B.P., the offset is about the same, 2,130 years ($\Delta^{14}C$ of 247 ± 20 per mil). However, by 11,050 years B.P., the offset has diminished to 1,060 years ($\Delta^{14}C$ of 97 ± 14 per mil), a value similar to that observed for the next several thousand years (2, 3). Over a period of 1,280 years between 12,330 and 11,050 years B.P., radiocarbon ages only diminish by about 210 years. Within error, the Huon Peninsula data from 13 to 11 ka are consistent with the Barbados data (22) (Figs. 4 and 5), which indicates that coral analyses are reproducible from two localities with different diagenetic environments and potentially different reservoir effects. Because of their smaller analytical errors and higher sample density, the Huon Peninsula data suggest that there was a large $\Delta^{14}C$ decrease (150 ± 24 per mil) within a short time interval (1280 ± 70 years). The decrease and the PRM were synchronous (Fig. 5), suggesting that the decrease was related to global melt rates. The decrease is the most prominent feature in the record of atmospheric $^{14}C/^{12}C$ variations over the last 20,000 years and represents almost two-thirds of the total lowering of atmospheric $\Delta^{14}C$ between 19 and 11 ka (Fig. 5) (36).

A change in ^{14}C production in the upper atmosphere, which changes the average $\Delta^{14}C$ of the combined atmosphere, ocean, and biosphere, could be caused by a change in either the terrestrial or solar magnetic fields. The latter is difficult to rule out because we have no direct way of obtaining independent records of the solar magnetic field. It is clear, however, that a simple relation among sun, climate, and $\Delta^{14}C$, as has been discussed for the Maunder Minimum (37), does not hold for the YD. For most of the last 20,000 years, there appears to have been an anticorrelation between the Earth's magnetic-dipole intensity (38, 39) and atmospheric $\Delta^{14}C$: Thus, millennial-scale fluctuations in $\Delta^{14}C$ may have resulted from changes in the intensity of the terrestrial magnetic dipole (2, 3, 9). However, the most prominent decrease in the $\Delta^{14}C$ record (Fig. 5) does not correspond to a comparably prominent increase in the magnetic record, which suggests that changes in the terrestrial magnetic field did not cause most of the decrease. Furthermore, the large average rate of the atmospheric $\Delta^{14}C$ decrease (117 ± 20 per mil per thousand years) is about the rate at which the average $\Delta^{14}C$ of the ocean-atmosphere system would decrease if ^{14}C production stopped completely. Thus, the rapidity of the decrease implicates a mechanism that does not involve production changes alone.

Because the ocean contains 95% of the exchangeable carbon in the ocean, atmosphere, and biosphere, nonproduction-related changes in atmospheric $\Delta^{14}C$ are most probably related to changes in the ocean. One manifestation of a perturbation in the carbon cycle is the rise in the atmospheric CO_2 concentration during the last deglaciation, which is documented by measurements of CO_2 in ice cores (40). Box models indicate that such a rise in CO_2 could be accompanied by a decrease in atmospheric $\Delta^{14}C$ of 25 to 75 per mil (9, 41). Although dating uncertainties preclude detailed correlation with the decrease in $^{14}C/^{12}C$ that is inferred from the Huon Peninsula corals, the ice-core data show that the change in CO_2 may not have been unidirectional during deglaciation and that some of the net glacial-interglacial rise in CO_2 concentration could have taken place at about the YD interval. Thus, some but not all of the $\Delta^{14}C$ decrease may have resulted from ocean-circulation changes associated with an atmospheric CO_2 increase.

An increase in the mixing rate of the ocean causes the average $\Delta^{14}C$ of the ocean to rise and the average $\Delta^{14}C$ of the combined atmosphere and biosphere to fall. Box models indicate that an increase by a factor of 2 in the ventilation rate produces a decrease in atmospheric $\Delta^{14}C$, at steady state, of several tens of per mil (42). Our melt rates (Fig. 3) suggest the presence of a mechanism that changes the ventilation rate. As melt rates decreased during the YD, North Atlantic surface-water salinity increased, causing an increase in NADW production. If global deep-ocean circulation paralleled NADW production, the rate of ocean ventilation increased and atmospheric $\Delta^{14}C$ decreased. When melt rates increased after the YD, the ventilation rate decreased, arresting the $\Delta^{14}C$ decrease. The coincidence of reduced global melting and the $\Delta^{14}C$ decrease (Fig. 5) supports this scenario. We suggest that this changing partitioning of ^{14}C between the atmosphere and the ocean was superimposed on the gradual lowering of average $\Delta^{14}C$ that was caused by the increasing intensity of the Earth's magnetic-dipole field strength between 20 and 10 ka (Fig. 5).

Previous studies have reconstructed certain aspects of past oceanic circulation. Combined measurements of $^{14}C/^{12}C$ in planktonic and benthic foraminifera from the same deep-sea sediment strata (42, 43) indicate that the ventilation rate was lower in the glacial ocean than in today's ocean. The ventilation rate about 10,000 ^{14}C years ago may have been somewhat higher than the present rate (42). However, more detailed work on the interval between 13 and 11 ka may be required to test whether the $\Delta^{14}C$ decrease was caused by a change in the ventilation rate. Certainly the possibility of a ventilation-rate change by a factor of 2 or more at about the time of the YD cannot be ruled out. Significant changes in ocean circulation, which largely involved changes in the rate of formation of NADW and lower North Atlantic Deep Water (LNADW) took place (44–46) before and during the YD. At least some of the changes appear to relate directly to climate in the vicinity of the North Atlantic. In some form and at some rate, formation of NADW continued before and throughout the YD (45, 46). Sarthein and colleagues (46) demonstrated that the rate of NADW formation before the YD was slower than it is now and faster than the present rate at some time during the YD, which is consistent with our inferences from the ^{14}C record. Although their study did not focus specifically on the YD interval, Duplessy and co-workers (47) showed that ventilation rates for short periods during deglaciation were two to three times higher than present rates. The inferred high rate of NADW formation at the end of the YD appears to conflict with cadmium data (48). However, this difference can be reconciled if NADW was more shallow at the end of the YD than at present height or if the ventilation rate of the ocean is not proportional to the rate of NADW production.

Meltwater input or diversion was a plausible trigger for the YD. During the YD, glacial melting slowed and atmospheric $\Delta^{14}C$ dropped dramatically, for approximately 1280 years, until several hundred years after the end of the YD. We infer from the abrupt decrease in atmospheric $\Delta^{14}C$ and its coincidence with slower rates of melting that the ventilation rate of the ocean was higher during this 1280-year interval, which is consistent with rates of NADW formation inferred from one other line of evidence (46). There is some uncertainty in the precise temporal relation between this interval and the YD (35) (Fig. 5). With errors taken into consideration, the PRM may have overlapped with the end of the YD by as much as 900 years or as little as 400 years. In either case, despite low globally averaged rates of meltwater input, apparently high rates of NADW formation, and rapid ocean ventilation, the climate in the North Atlantic region remained cool during the late YD. One explanation for this apparent discrepancy includes the possibility (45) that the North Atlantic climate during the YD was controlled not by the global circulation rate or even by the rate of formation of NADW but by the rate of formation of LNADW. The rate of LNADW formation, in turn, may have been controlled not by globally averaged rates of melting but by meltwater discharge from the Fennoscandian ice sheet. A second possibility is that NADW

formed and released heat at lower latitudes during the late YD.

REFERENCES AND NOTES

1. W. F. Libby, *Radiocarbon Dating* (Univ. of Chicago Press, Chicago, 1952); H. de Vries, *Proc. K. Ned. Akad. Wet. B* **61**, 94 (1958).
2. M. Stuiver and R. S. Kra, Eds., *Radiocarbon* **28**, 805 (1986).
3. B. Becker and B. Kromer, *ibid.*, p. 961.
4. _____, P. Trimborn, *Nature* **353**, 647 (1991).
5. A. Kaufman and W. S. Broecker, *J. Geophys. Res.* **70**, 4039 (1965).
6. J. H. Chen, R. L. Edwards, G. J. Wasserburg, *Earth Planet. Sci. Lett.* **80**, 241 (1986).
7. R. L. Edwards, J. H. Chen, G. J. Wasserburg, *ibid.* **81**, 175 (1987); R. L. Edwards, J. H. Chen, T.-L. Ku, G. J. Wasserburg, *Science* **236**, 1547 (1987); R. L. Edwards, F. W. Taylor, G. J. Wasserburg, *Earth Planet. Sci. Lett.* **90**, 371 (1988); R. L. Edwards, thesis, California Institute of Technology (1988).
8. R. G. Fairbanks, *Nature* **342**, 637 (1989).
9. E. Bard, B. Hamelin, R. G. Fairbanks, A. Zindler, *ibid.* **345**, 405 (1990).
10. M. Stuiver, T. F. Braziunas, B. Becker, B. Kromer, *Quat. Res.* **35**, 1 (1991).
11. W. S. Broecker, *Paleoceanography* **5**, 459 (1990).
12. J. M. A. Chappell and H. A. Pollach, *Nature* **349**, 147 (1991).
13. We calculated the rate of tectonic uplift at the drilling site by assuming that the last interglacial terrace [Terrace VIIb; J. M. A. Chappell, *Geol. Soc. Am. Bull.* **85**, 553 (1974); A. L. Bloom, W. S. Broecker, J. M. A. Chappell, R. K. Matthews, K. J. Mesollela, *Quat. Res.* **4**, 185 (1974)] near the drilling site originally formed 6 m above present sea level [T.-L. Ku, M. A. Kimmel, W. H. Easton, T. J. O'Neil, *Science* **183**, 959 (1974)]. Because the present elevation of Terrace VIIb is 243 m and the average age of the last interglacial terraces dates to about 125,000 years ago (*7*), the uplift rate averaged over the last 125,000 years is 1.9 m per thousand years. The assumption of constant uplift rate appears to be valid for the Huon Peninsula [A. L. Bloom and N. Yonekura, *Models in Geomorphology*, M. J. Woldenberg, Ed. (Allen and Unwin, Winchester, MA, 1985), p. 139]. For the ^{14}C curve in Fig. 2, the age used in the uplift correction was the ^{230}Th age or, if this value was not determined, the calendar age on the basis of the ^{14}C calibration (Fig. 5).
14. The ^{14}C ages are calculated on the assumption of an initial $^{14}C/^{12}C$ ratio that corresponds to a value of 0 for $\Delta^{14}C$ (*30*). The abbreviation B.P. stands for before present, where the present is taken to be the year 1950 A.D.
15. P. J. Slota, Jr., A. J. T. Jull, T. W. Linick, L. J. Toolin, *Radiocarbon* **29**, 303 (1987); T. W. Linnick, A. J. T. Jull, L. J. Toolin, D. J. Donahue, *ibid.* **28**, 961 (1986); D. J. Donahue, A. J. T. Jull, L. J. Toolin, *Nucl. Instrum. Methods Phys. Res. B* **52**, 224 (1990).
16. D. J. Donahue, T. W. Linick, A. J. T. Jull, *Radiocarbon* **32**, 135 (1990).
17. G. S. Burr, R. L. Edwards, D. J. Donahue, E. R. M. Druffel, F. W. Taylor, *ibid.* **34**, 611 (1992).
18. We measured the $\delta^{13}C$ for all samples and used these values to correct measured $^{14}C/C$ ratios (at Woods Hole) or measured $^{14}C/^{13}C$ ratios (at Arizona) for fractionation.
19. S. Griffin and E. R. M. Druffel, *Radiocarbon* **27**, 43 (1985). Data are reported as specified in (*31*); reported errors are a combination of counting-statistics and laboratory random errors.
20. J. M. A. Chappell and H. A. Pollach, *Quat. Res.* **2**, 244 (1972).
21. In (*17*), levels of natural contamination were documented and correspond to shifts in ^{14}C age of less than 200 years to 2100 years for coral that is 20,000 years old. The average $\Delta^{14}C$ of the Barbados samples with ^{230}Th ages between 15,000 and 25,000 years is 430 per mil without selective dissolution and 350 per mil with selective dissolution [determined by the averaging of points in tables 1A and 1B in (*22*)]. This corresponds to a difference in ^{14}C age of 460 years. If one chooses a pair of analyses for a single Barbados sample in this age range, the $\Delta^{14}C$ value determined with selective dissolution (*22*) is typically lower than the value determined without selective dissolution (*9*); however, the two values typically agree within 2σ analytical errors.
22. E. Bard, M. Arnold, R. G. Fairbanks, B. Hamelin, *Radiocarbon* **35**, 191 (1993).
23. J. L. Banner, G. J. Wasserburg, J. H. Chen, J. D. Humphrey, *Earth Planet. Sci. Lett.* **107**, 129 (1991); E. Bard, R. G. Fairbanks, B. Hamelin, A. Zindler, C. T. Hoang, *Geochim. Cosmochim. Acta* **55**, 2385 (1991); B. Hamelin, E. Bard, R. G. Fairbanks, A. Zindler, *Earth Planet. Sci. Lett.* **106**, 169 (1991).
24. C. D. Gallup, R. L. Edwards, R. G. Johnson, *Eos* **72**, 271 (1991).
25. The Finnigan MAT 262–RPQ at the Minnesota Isotope Laboratory is specifically configured to measure small ion beams. Ions were detected before the static-quadrupole second stage with the use of an electron multiplier in its ion-counting mode. This instrument has ion-counting efficiency greater than 90%, a dark noise of 0.05 counts per second, and no reflected beams larger than 10^{-8} times the intensity of the primary beam. Uranium is loaded on a rhenium filament without graphite and is run with the double-filament technique.
26. The NBL Standard Reference Material 112a is a high-purity uranium metal formerly called National Bureau of Standards Standard Reference Material 960.
27. The $\delta^{234}U$ value is the fractional difference between the measured $^{234}U/^{238}U$ ratio and the $^{234}U/^{238}U$ ratio at secular equilibrium, in parts per thousand. It is equal to

$$\{[(^{234}U/^{238}U)_{measured}/(^{234}U/^{238}U)_{se}] - 1\} \times 1000$$

The value of $^{234}U/^{238}U$ at secular equilibrium is $\lambda_{238}/\lambda_{234} = 5.472 \times 10^{-5}$, where λ represents each respective decay constant (see Table 1) (*49*). Initial $\delta^{234}U$ values are equal to $(\delta^{234}U_{measured})(e^{\lambda 234 T})$, where T is the ^{230}Th age defined in Table 1.
28. J. H. Chen, H. A. Curren, B. White, G. J. Wasserburg, *Geol. Soc. Am. Bull.* **103**, 82 (1991); M. Stein, G. J. Wasserburg, K. Lajoie, J. H. Chen, *Geochim. Cosmochim. Acta.* **55**, 3709 (1991); S. J. Goldstein, M. T. Murrell, D. R. Janecky, J. R. Delaney, D. A. Clague, *Earth Planet. Sci. Lett.* **107**, 25 (1991).
29. A. N. Dia, A. S. Cohen, R. K. O'Nions, N. J. Shackleton, *Nature* **356**, 786 (1992).
30. The $\Delta^{14}C$ value is the per mil difference between the initial $^{14}C/^{12}C$ of a sample (normalized for isotope fractionation) and the $^{14}C/^{12}C$ of a standard; the standard has a value similar to the initial $^{14}C/^{12}C$ ratio of 19th century wood. The $\Delta^{14}C$ value is defined and discussed in (*31*) and equals $(Fe^{\lambda T} - 1) \times 1000$ per mil, where F is the fraction modern (*16*), λ is the decay constant that corresponds to the 5730-year half-life, and T is the age in calendar years B.P. In this report, $\Delta^{14}C$ is calculated by the correction of the measured $^{14}C/^{12}C$ ratio for the reservoir effect, and then the calculation of the initial $^{14}C/^{12}C$ ratio with the use of the ^{230}Th age. Quoted errors include errors in the measured $^{14}C/^{12}C$ ratio, the reservoir effect, and the ^{230}Th age.
31. M. Stuiver and H. Polach, *Radiocarbon* **19**, 355 (1977).
32. T. W. Linick, A. Long, P. E. Damon, C. W. Ferguson, *ibid.* **28**, 943 (1986); M. Stuivev and G. W. Pearson, *ibid.*, p. 805.
33. W. F. Ruddiman, in *North American and Adjacent Oceans during the Last Deglaciation*, vol. K-3 of *The Decade of North American Geology*, W. F. Ruddiman and H. E. Wright, Jr., Eds. (Geological Society of America, Boulder, CO, 1987), pp. 137–154 and 463–478.
34. See W. S. Broecker *et al.*, *Paleoceanography* **3**, 1 (1988) and references therein.
35. On the basis of ^{14}C dating of lacustrine and marine sediments, the YD started between 11,200 and 11,000 ^{14}C years B.P. and ended between 10,200 and 10,000 ^{14}C years B.P. [N. K. Karpuz and E. Jansen, *Paleoceanography* **7**, 499 (1992) and references therein], although dates as old as 10,500 ^{14}C years B.P. (*45*) have been reported for the end of the YD. Because the end of the YD and the $^{14}C/^{12}C$ drop occurred at about the same time, when the ^{14}C age of the end of the YD is translated into calendar years the uncertainty in the calendar age is large (Fig. 4) (10,000 to 10,400 ^{14}C years B.P. corresponds to 11,000 to 12,500 calendar years B.P.). Therefore, in comparing our records to those for the YD, we have relied on ice-core dating. On the basis of the counting of annual layers, the oxygen isotope and conductivity anomalies associated with the YD lie between 12,940 ± 260 and 11,640 ± 250 years B.P.; the duration of the YD is 1300 ± 70 years [R. B. Alley *et al.*, *Eos* **73**, 259 (1992); R. B. Alley *et al.*, *Nature* **362**, 527 (1993); independent ice-core dates from S. J. Johnsen *et al.*, *ibid.* **359**, 311 (1992) are consistent with these values].
36. The atmospheric $\Delta^{14}C$ value at about 18.7 ka is from analyses of RGF9-21-11, RGF9-24-04, and RGF9-27-5 (*22*). The age of 18.7 ka is the mean of the ^{230}Th ages of the first two samples and the most precise age (analysis 1) of the third sample. The $\Delta^{14}C$ value of 342 ± 41 per mil is the average of the $\Delta^{14}C$ of the latter two samples and the average of the two $\Delta^{14}C$ values (based on radiocarbon analyses 1 and 2) of the first sample.
37. J. A. Eddy, *Science* **192**, 1189 (1976). The Maunder Minimum was characterized by a small sunspot number, a large atmospheric $\Delta^{14}C$, and a cool climate, all of which are qualitatively consistent with a small solar constant (causing cool climate and a corresponding small solar magnetic field). Because the YD was characterized by a decreasing $\Delta^{14}C$ and a cool climate, such a simple scenario does not apply to it.
38. D. Walton, *Nature* **310**, 740 (1984); L. Tauxe and J.-P. Valet, *Phys. Earth Planet. Inter.* **56**, 59 (1989); M. W. McElhinny and W. E. Senanayake, *J. Geomagn. Geoelectr.* **34**, 39 (1982).
39. E. Tric *et al.*, *J. Geophys. Res.* **97**, 9337 (1992).
40. W. Berner, H. Oeschger, B. Stauffer, *Radiocarbon* **22**, 227 (1980); B. Stauffer, H. Hofer, H. Oeschger, J. Schwander, U. Siegenthaler, *Ann. Glaciol.* **5**, 160 (1984); J. M. Barnola, D. Raynaud, Y. S. Korotkevich, C. Lorius, *Nature* **329**, 408 (1987); R. J. Delmas, J.-M. Ascencio, M. Legrand, *ibid.* **284**, 155 (1980); see also summary figure in M. Leuenberger, U. Siegenthaler, C. C. Langway, *ibid.* **357**, 488 (1992) and references therein.
41. U. Siegenthaler, M. Heimann, H. Oeschger, *Radiocarbon* **22**, 177 (1980); R. S. Keir, *Earth Planet. Sci. Lett.* **64**, 445 (1983); D. Lal and R. Revelle, *Nature* **308**, 344 (1984).
42. M. Andree *et al.*, *Clim. Dyn.* **1**, 53 (1986).
43. W. S. Broecker *et al.*, *Paleoceanography* **3**, 659 (1988); N. J. Shackleton *et al.*, *Nature* **335**, 708 (1988).
44. T. Veum, E. Jansen, M. Arnold, I. Beyer, J.-C. Duplessy, *Nature* **356**, 783 (1992).
45. S. J. Lehman and L. D. Keigwin, *ibid.*, p. 757.
46. M. Sarnthein, K. Winn, J.-C. Duplessy, L. Labeyrie, H. Erlenkeuser, *Fourth International Conference on Paleoceanography, Program and Abstracts* (1992), p. 248.
47. J.-C. Duplessy *et al.*, *Earth Planet. Sci. Lett.* **103**, 27 (1991).
48. L. D. Keigwin, G. A. Jones, S. J. Lehman, E. A. Boyle, *J. Geophys. Res.* **96**, 16811 (1991).
49. Values for decay constants are: $\lambda_{238} = 1.551 \times 10^{-10}$ year^{-1} [A. H. Jaffey, K. F. Flynn, L. W. Glendenin, W. C. Bentley, A. M. Essling, *Phys. Rev. C* **4**, 1889 (1971)], $\lambda_{234} = 2.835 \times 10^{-6}$ year^{-1} [M. Lounsbury and R. W. Durham, in *Proceedings of the International Conference on Chemical Nuclear Data, Measurements and Applications*, M. L. Hurrell, Ed. (Institute of Civil Engineers, London, 1971), p. 215; P. de Bievre *et al.*, in *ibid.*, p. 21], and $\lambda_{230} = 9.195 \times 10^{-6}$ year^{-1} [J. W. Meadows, R. J. Armani, E. L. Callis,

A. M. Essling, *Phys. Rev. C* 22, 750 (1980)].
50. We thank the other members of the New Guinea field expedition of 1988, particularly E. Wallensky who facilitated all aspects of the field research; M. Stuiver, E. A. Boyle, S. J. Lehman, D. Lea, K. Kelts, H. E. Wright, Jr., T. Brazuinas, B. Haskell, M. Abbott, C. D. Gallup, D. A. Richards, and two anonymous reviewers for helpful comments and discussions; and J.W.B. for important contributions to the interpretation of our data. Supported by National Science Foundation (NSF) grants EAR-8804970 (A.L.B.), EAR-8904705 (R.L.E.), ATM-8904987 (F.W.T.), OCE-8915919 (E.R.M.D.), and ATM-8921760 (R.L.E.); and, for the TIMS analytical facility, by NSF grant EAR-8817260 (R.L.E.) and the University of Minnesota.

22 December 1992; accepted 19 April 1993

Beach Cusps as Self-Organized Patterns

B. T. Werner and T. M. Fink

Computer simulations of flow and sediment transport in the swash zone on a beach demonstrate that a model that couples local flow acceleration and alongshore surface gradient is sufficient to produce uniformly spaced beach cusps. The characteristics of the simulated cusps and the conditions under which they form are in reasonable agreement with observations of natural cusps. The self-organization mechanism in the model is incompatible with an accepted model in which standing alongshore waves drive the regular pattern of erosion and deposition that gives rise to beach cusps. Because the models make similar predictions, it is concluded that currently available observational data are insufficient for discrimination between them.

Beach cusps are uniformly spaced, arcuate scallops in sediment that form at the shoreward edge of the episodically exposed portion of a beach known as the swash zone. Beach cusps and other regular topographic features in the nearshore, including ripples, megaripples, sand bars, ridges and runnels, sand waves, and swash marks (*1*), have attracted investigation owing to their beauty, their effect on sediment transport, and their uniformity in the presence of complex interactions between waves, currents, and sediment. According to a widely accepted hypothesis, the form and spacing of beach cusps reflect a pattern of alongshore standing waves on the beach (*2–4*). An alternative, physically incompatible model ascribes cusp formation to feedback between swash flow and beach morphology. This model has been discounted partially because of the difficulty of understanding how local interactions between fluid and sediment lead to globally uniform patterns (*4*). Using computer simulations, we show that uniform beach cusps can develop by local flow-morphology feedback, examine the implications of this self-organization model, and demonstrate that the predictions of the standing wave and self-organization models are sufficiently similar that current data and observations cannot distinguish unambiguously between them.

Beach cusps form on oceanic and lacustrine beaches and in sediments ranging from fine sand to cobbles. They result from a varying combination of accretion at cusp horns and erosion in the interjacent cusp bays (*1*). Cusps are typically spaced 10 cm to 60 m apart (*1*). Beach cusp formation is favored under conditions of surging, nonbreaking waves of near-normal incidence on steep (usually coarse-grained) beaches (*1, 5*). Swash runs up a beach without cusps as a thinning, often irregular sheet. On a cuspate beach, runup is deflected by horns toward bays and from there flows seaward as runout.

In the self-organization model, incipient topographic depressions in a beach are amplified by attracting and accelerating water flow, thereby enhancing erosion (Fig. 1A) (*5*). Dean and Maurmeyer (6) related well-developed beach cusp spacing to the swash excursion, the horizontal distance between the highest and lowest positions of the swash front on a beach, by considering the kinematical trajectory of elastic particles sliding on the surface of a cusp.

In contrast, according to the standing-wave model, the pattern of erosion and deposition of sediment leading to beach cusps originates with the flow patterns of alongshore standing waves (*2–4, 7, 8*), generally taken to be subharmonic edge waves (Fig. 1B), which are trapped waves with half the frequency of incident waves. The standing wave model successfully predicts beach cusp spacing as a function of incident wave frequency and beach slope within about a factor of 2 (*4, 9*) (compatible with uncertainties in model input parameters). In addition, standing waves induce cusp formation in sand at the swash zone margin on a laboratory concrete beach (*3*). However, because subharmonic edge waves decay strongly within one incident wavelength of the shore, they are difficult to detect. Standing subharmonic edge waves have not been observed unambiguously in conjunction with beach cusp formation in the field (*10*).

Our simulation algorithm uses a simplified model of coupled flow, sediment transport, and morphology change with the goal of simulating the evolution of cusps from arbitrary initial morphology. In contrast, earlier models considered wave and fluid flow interactions with a plane (*3, 7*) or a regular cuspate beach (*6, 8*) only. We are able to investigate the development of uniform cusps, rather than postulating their uniformity and general form, and to simulate explicitly conditions under which cusps do not form.

Our model treats only the kinematics in gravity of swash flow over a beach (*6*), without directly considering the hydrodynamics of swash. This approximation is supported by an inviscid calculation (*11*) and laboratory measurements (*12*) on the motion of the swash front (the leading edge of the swash). Flow is simulated by cubical water particles, representing the swash front, that move according to Newton's laws in gravity (the kinematical equations) and are constrained to remain on the surface of the beach. For example, water particles move on parabolas in the swash zone on a plane beach (Fig. 2A). In addition to the gravitational force, water particles are repelled from regions of high water particle concentration and are attracted toward regions of low concentration in a simplified approximation to flow caused by pressure gradients induced by the sea surface.

The simulated beach is composed of thin, square slabs of sediment stacked on a rectangular grid of square cells with periodic

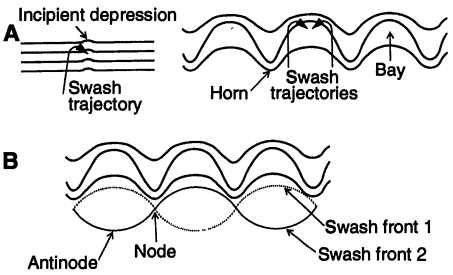

Fig. 1. Self-organization and standing wave models. Seaward is down. Bold lines are beach contours. (**A**) (Left) Deflection of swash flow by incipient topographic depression causing further erosion; (right) swash zone circulation in equilibrium with beach cusps (*6*). (**B**) Alignment of beach cusps and sinusoidal variation in the swash front caused by subharmonic edge waves shown at two consecutive swash cycles as broken and solid lines (*3*). Nodes in the swash excursion align with cusp horns.

B. T. Werner, Center for Coastal Studies, Scripps Institution of Oceanography, La Jolla, CA 92093–0209.
T. M. Fink, Division of Physics, Mathematics and Astronomy 200-36, California Institute of Technology, Pasadena, CA 91125.